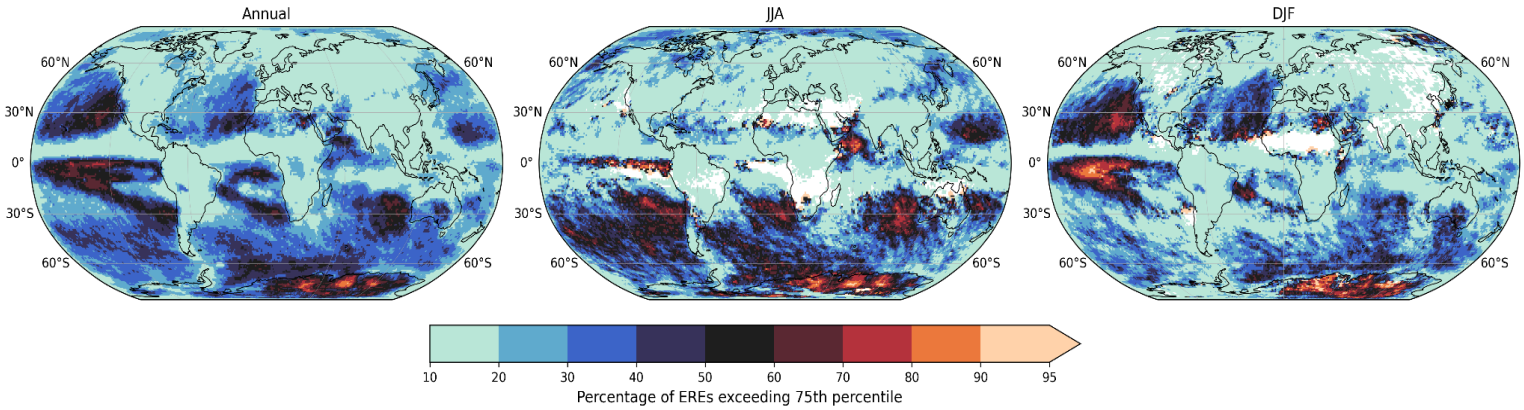

Figure S1. Percentage of EREs exceeding the 75th percentile of ERE size. The 75th percentile is defined globally using (1) annual data, (2) JJA, and (3) DJF, separately for the plots above. Figures and tables present analyses for the study period 1980–2020 unless stated otherwise.

Dataset	Annual	JJA	DJF
MSWEP	1.50	1.47	1.36
GPCP	1.58	1.71	1.60
IMERG	1.56	1.62	1.55

Table S1. Table showing the ocean-to-land ERE size ratio for different seasons using multiple observational datasets.

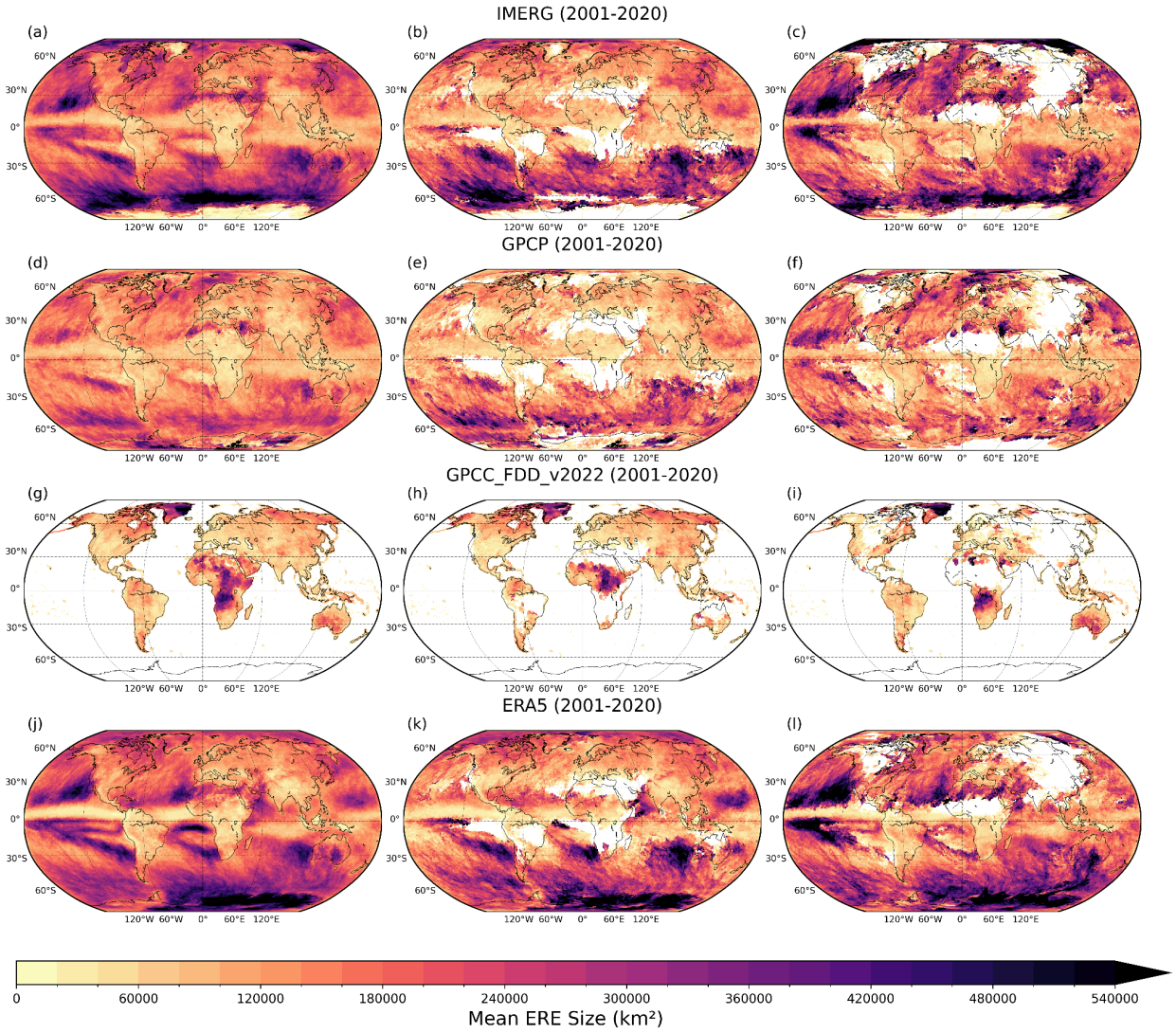

Figure S2. ERE sizes from different datasets for the period 2001–2020: (a–c) IMERG, (d–f) GPCP, (g–i) GPCC, and (j–l) ERA5. The first column shows the annual average, the second column shows the boreal summer (JJA) average, and the third column shows (DJF) average.

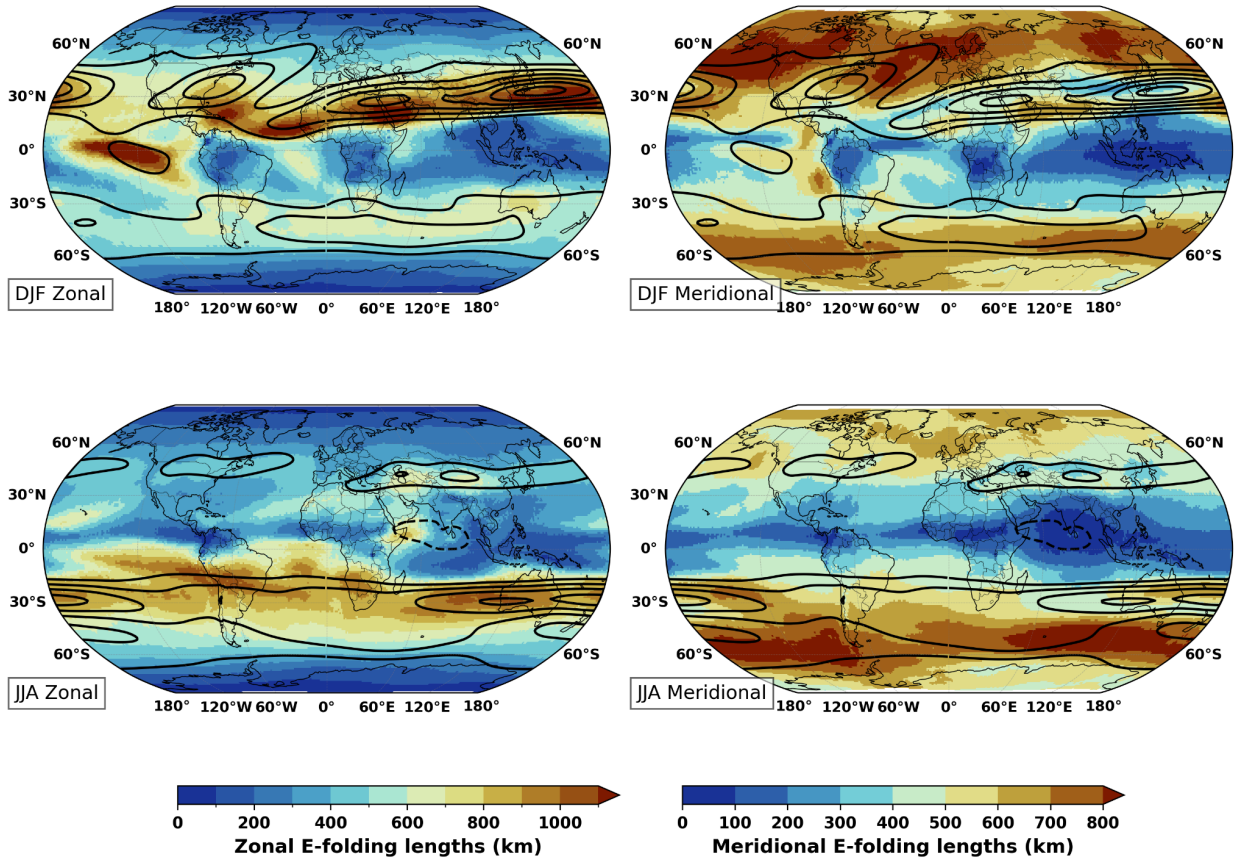

Figure S3. Zonal and meridional e-folding length scales. Wind speed contours, representing the subtropical jetstream, are shown for values exceeding 20 m s^{-1} (plotted at 10 m s^{-1} intervals). Negative contours for values exceeding 20 m s^{-1} are shown as dashed lines. The first row corresponds to December–February (DJF), and the second row to June–August (JJA). The first column shows zonal e-folding length scales, and the second column shows meridional e-folding length scales.

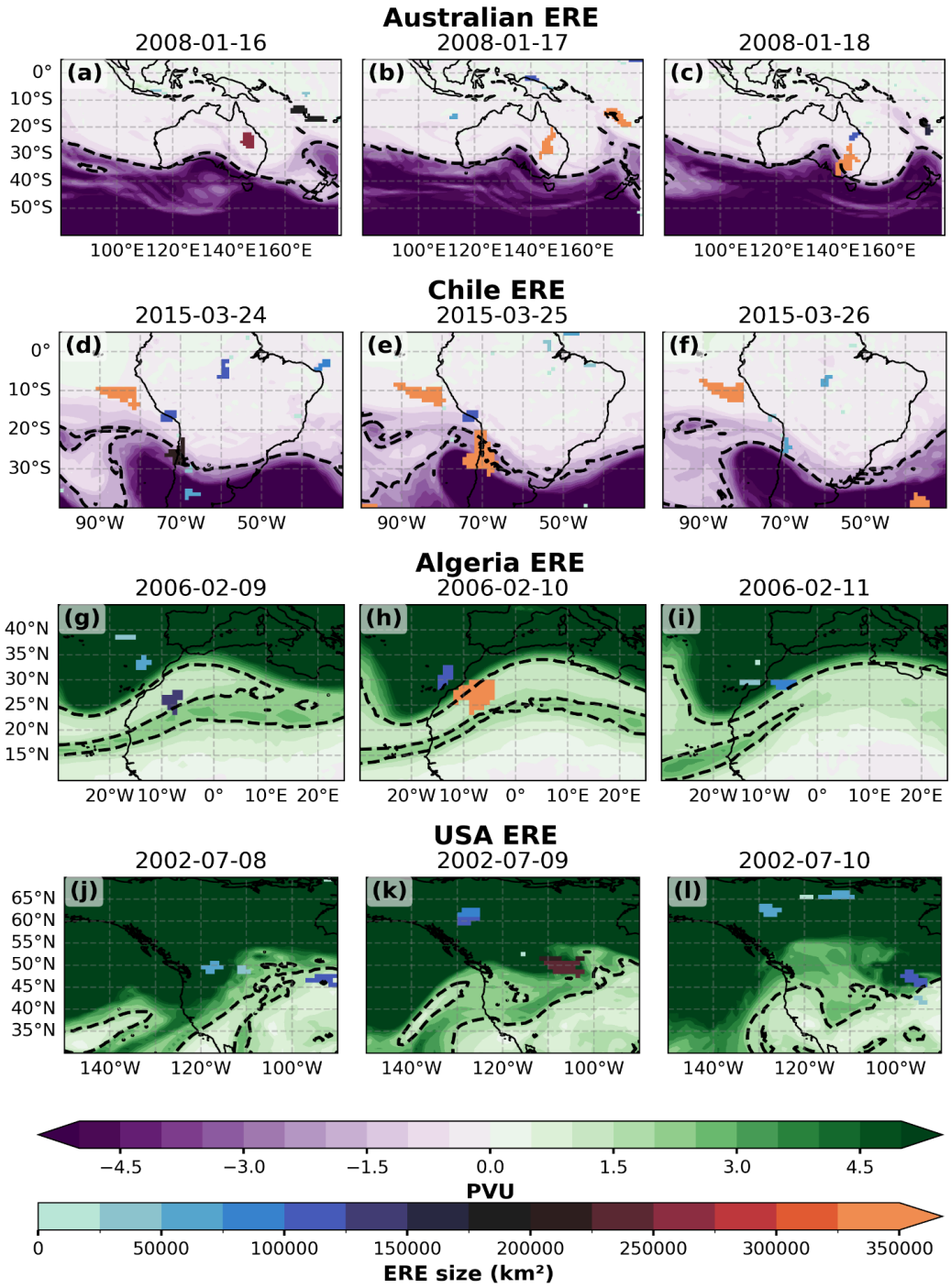

Figure S4. Case studies of large precipitation extremes in land hotspot regions. The examples are selected from the Emergency Events Database (EM-DAT, https://www.emdat.be/). The background shading indicates the Potential vorticity, where a 2 PVU contour is shown using a dotted black line. The spatial footprint of ERE (in km^2) is shown using a blue-red ('IceFire' proplot colormap).

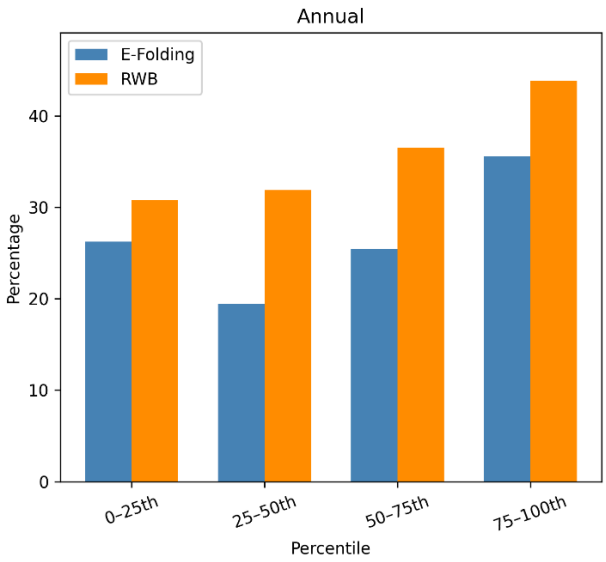

Figure S5. Probability of EREs associated with Rossby wave breaking events (RWB, orange bars) and regions of high e-folding length (blue bars). An ERE is considered associated with RWB if it occurs within 500 km of an RWB event, with probabilities calculated for the extratropics (30°–90° N/S). High e-folding regions are defined as grid points exceeding the local 75th percentile, and probabilities are computed as the fraction of EREs overlapping at least one such grid point across 90°S–90°N.

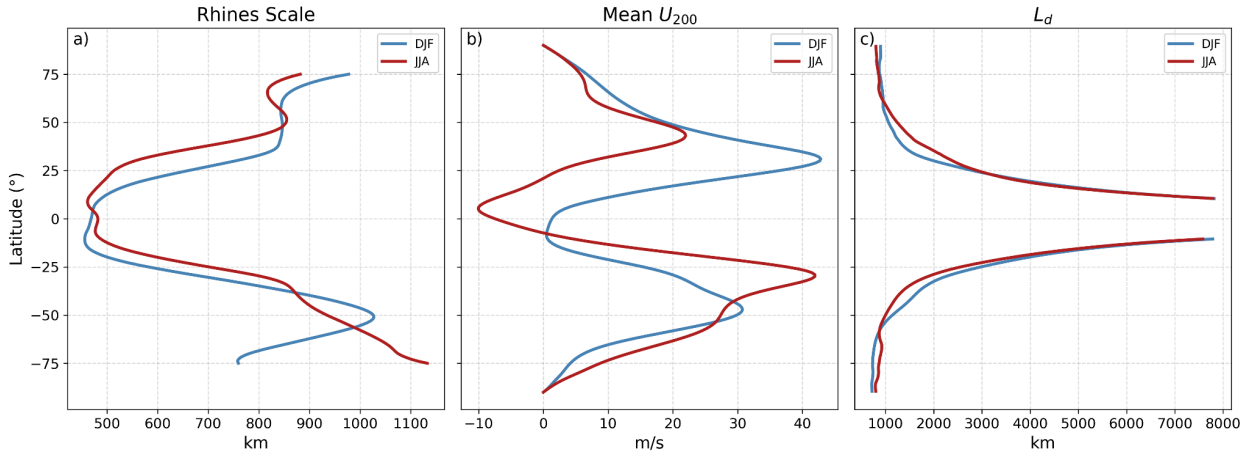

Figure S6. Zonal mean (a) Rhines scale (L_β), (b) mean zonal wind at 200 hPa, and (c) Rossby radius of deformation (L_d) for DJF (blue) and JJA (red).

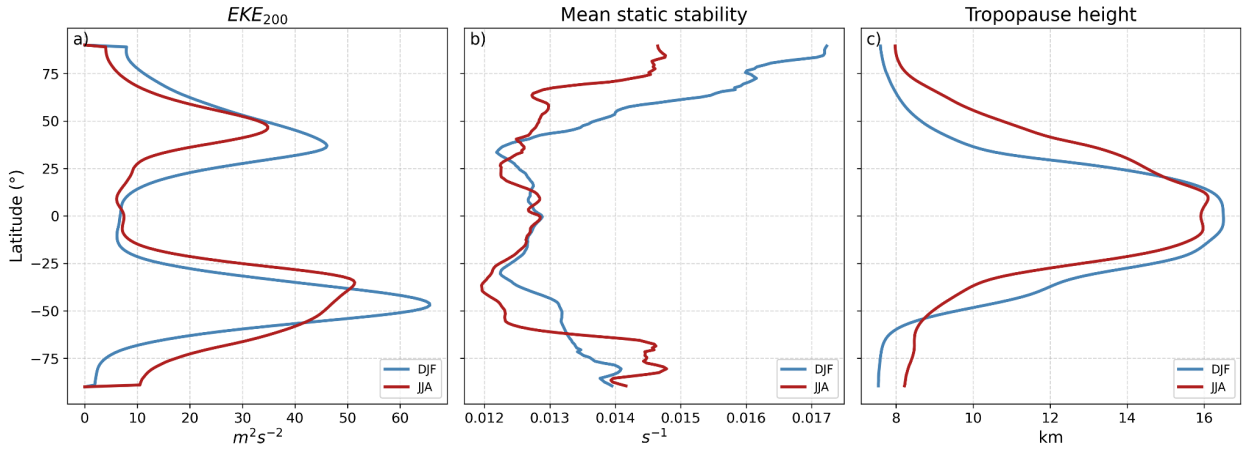

Figure S7. Zonal mean (a) EKE at 200hpa, (b) Mean static stability (N), and (c) Tropopause height (H) for DJF (blue) and JJA (red).

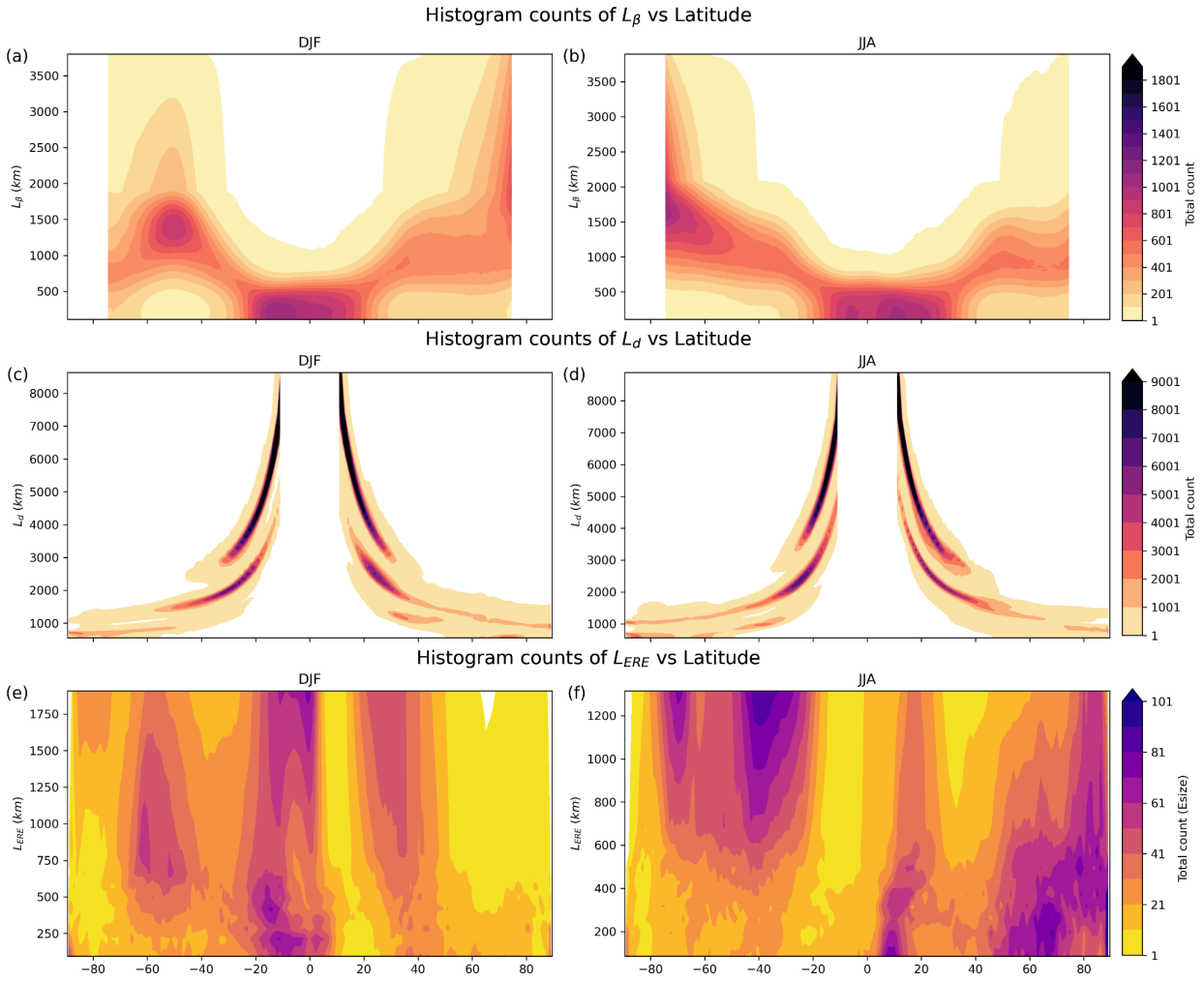

Figure S8. Histogram of (a, b) L_β, (c, d) L_d , and (e, f) L_{ERE} versus latitude. The first column corresponds to the DJF season, and the second column corresponds to the JJA season.

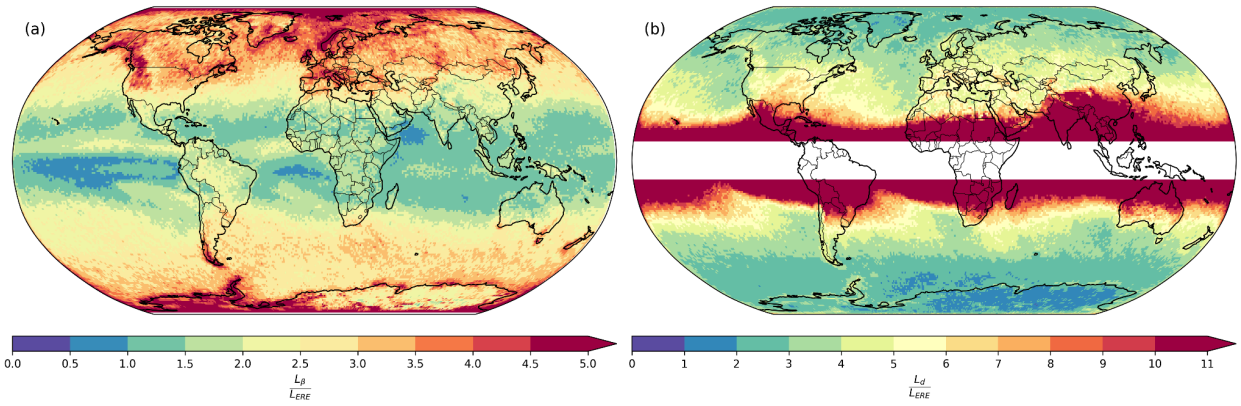

Figure S9. The mean ratio of the Rhines scale to the length scale of ERE ($\frac{L_\beta}{L_{ERE}}$, left panel), and of the Rossby radius of deformation to the length scale of ERE ($\frac{L_d}{L_{ERE}}$, right panel).

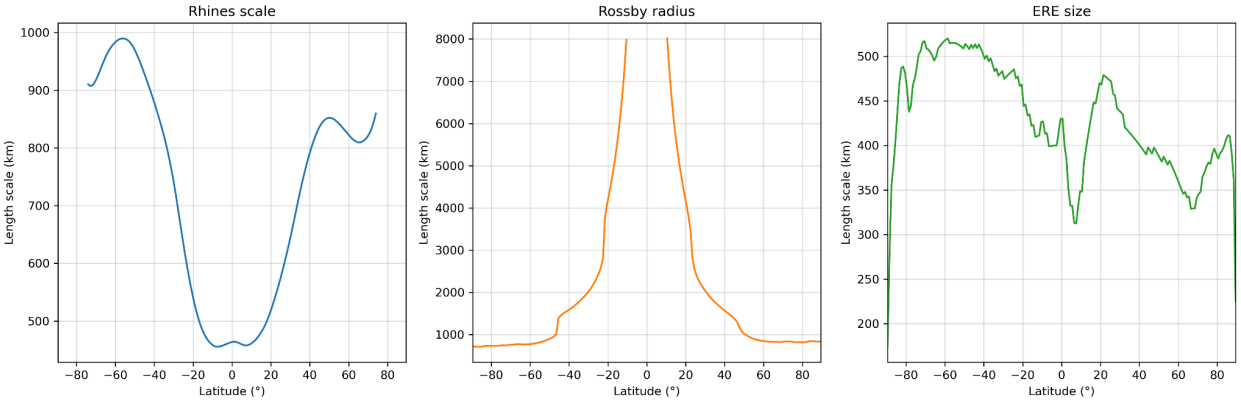

Figure S10. The median (50th percentile) values for L_β, L_d, and L_{ERE} across latitudes (left to right).

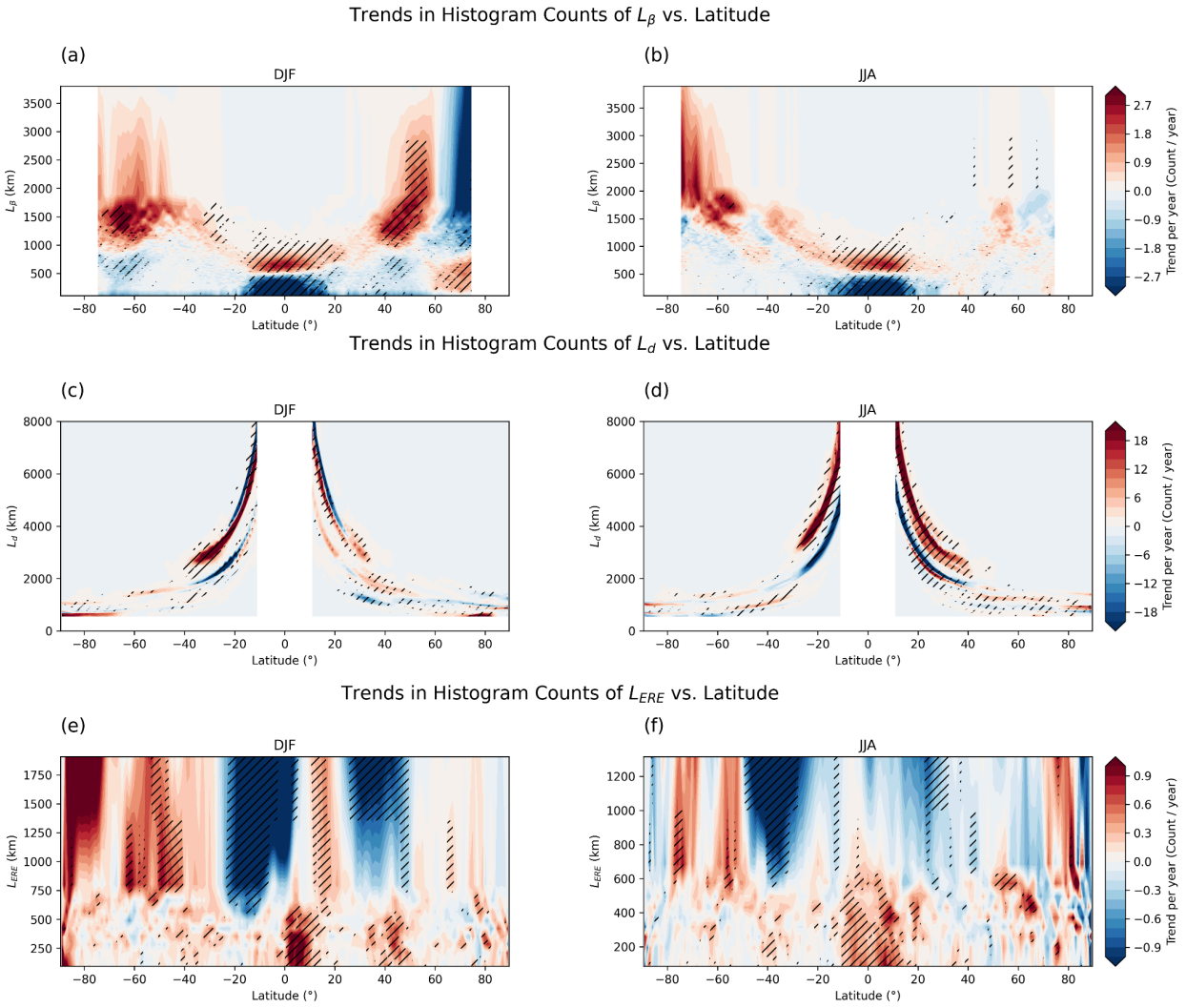

Figure S11. Trends in Histogram of (a, b) L_β, (c, d) L_d , and (e, f) L_{ERE} versus latitude. The first column corresponds to the DJF season, and the second column corresponds to the JJA season. The hatching indicates regions where the trend is significant ($p < 0.05$)